Materials Research. 2013; 16(6): 1254-1259
DOI: 10.1590/S1516-14392013005000136

Corrosion Behavior of HA-316L SS Biocomposites in Aqueous Solutions

***Alain Robin*[a]*, *Gilbert Silva*[b], *Jorge Luiz Rosa*[a]**

[a]*Departamento de Engenharia de Materiais, Escola de Engenharia de Lorena, Universidade de São Paulo – USP, CP 116, CEP 12600-000, Lorena, SP, Brazil*
[b]*Instituto de Engenharia Mecânica, Universidade Federal de Itajubá – UNIFEI, CEP 37500 903, Itajubá, MG, Brazil*

Received: February 18, 2013; Revised: April 19, 2013

316L stainless steel and Hydroxyapatite (5, 20 and 50 wt. (%) HA)-316L stainless steel composites were fabricated by mechanical alloying technique, pressing and sintering from 316L and HA powders. The corrosion behavior of both sintered 316L and HA-316L composites was evaluated by electrochemical techniques in simulated body fluid (Ringer's solution) and in 0.1M HCl solution which simulates occluded cell corrosion conditions. The results indicate that 316L stainless steel and HA-316L composites are passive in Ringer's solution and active in HCl solution. All materials are highly corrosion resistant in Ringer's solution with corrosion current density in the order of 10^{-6} A cm^{-2} or less. Both 316L stainless steel and 5% HA-316L composite present good corrosion resistance in HCl with corrosion current density in the order of 10^{-5} A cm^{-2}. The corrosion resistance decreases with increasing HA content in both solutions.

Keywords: *biocomposite, 316L SS, hydroxyapatite, corrosion*

1. Introduction

316L austenitic stainless steel (316L SS) is widely used as surgical implant material due to its biocompatibility, corrosion resistance and good mechanical strength[1]. Unfortunately, 316L steel only forms weak mechanical bond with the bone tissue due to its biological inertness, which turns difficult the fixing of implant to live bone. In order to improve the osseointegration of these implants, different studies were performed on the deposition of hydroxyapatite (HA) on stainless steel[2-5]. Indeed, HA ($Ca_{10}(PO_4)_6(OH)_2$) has a similar chemical composition and crystallographic structure as the natural apatite of human body bone and consequently can form strong bonds with the bone. Simultaneously, the HA coating helps to prevent the release of metal ions from the steel implant and their accumulation in the internal organs. Another alternative to improve the interaction between the steel implant and the bone is the development of 316L steel based biocomposites containing HA[6-10]. Fan et al.[9] studied the formation of bone-like apatite on HA/316L SS composites in simulated body fluid (SBF) and proved that the composites are excellent bioactive materials. Nevertheless, HA is brittle and the mechanical resistance of the HA-316L composites is lower than that of 316L stainless steel[7]. It is well known that stainless steels are generally passive in neutral media but are susceptible to pitting and crevice corrosion in chloride media. These forms of corrosion are associated to local acidification and generally lead to a severe localized active dissolution[11].

Tulinski[12,13] showed that HA addition improved the corrosion resistance of HA/ nitrided nickel-free austenitic stainless steel in Ringer's solution. No work was found about the corrosion resistance of HA/316L SS composites.

This work aimed to study the corrosion behavior of HA/316L SS biocomposites in simulated physiological solution (Ringer's solution) and under simulated occluded cell corrosion conditions (0.1M HCl). The investigation was based on electrochemical techniques.

2. Experimental

2.1. *Material*

HA powder was prepared by wet precipitation using $Ca(NO_3)_2.4H_2O$ and H_3PO_4 reagents, followed by filtration, calcination at 900 °C for 2 h and deagglomeration. The whole procedure of preparation was detailed elsewhere[14]. 316L stainless steel powder (size ranging from 5 to 30 μm) and HA powder were mixed in the following proportions, 95/5, 80/20 and 50/50 weight percent. The mixtures were homogenized for 10 h using a dry planetary ball mill (Fritsch, model Pulverisette 5) under the following conditions: stainless steel balls (18 mm-diameter) and vessel (250 mL), ball to powder mass ratio 10:1, speed 120 rpm. Then, the mixtures were uniaxially pressed under 32 MPa pressure and then isostatically pressed under 200 MPa pressure. The densified mixtures were heated under vacuum in a resistive furnace up to 1200 °C at a 10 °C/min rate, maintained at 1200 °C for 2 h and then naturally cooled to room temperature.

2.2. *Electrochemical study*

Cylindrical slices (of nearly 9 mm diameter and 3 mm thickness) were cut from the sintered 316L and HA-316L

*e-mail: alain@demar.eel.usp.br

composite rods and then mounted in resin. The cross-section of the electrodes (about 0.7 cm^2 area) was mechanically ground up to a 1200-grit finish, rinsed with distilled water and dried.

The electrolytic solutions used for the electrochemical study were the naturally aerated Ringer's solution (whose composition is: 8.6 g NaCl + 0.3 g KCl + 0.33 g $CaCl_2$-H_2O in 1000 mL deionized water) and the naturally aerated 0.1M HCl solution. The counter electrode was a square-shaped platinum sheet of 18 cm^2 area and the reference electrode was the saturated calomel electrode (SCE). The experiments were performed at room temperature.

Open-circuit potential, electrochemical impedance spectroscopy (EIS) and polarization measurements were made using the Electrochemical Interface SOLARTRON mod. 1287A and the Frequency Response Analyzer SOLARTRON mod. 1260 A, controlled by the Ecorr/Zplot SOLARTRON mod. 125587S software. Triplicate assays were performed and reproducibility was verified.

Prior to polarization experiments, the working electrodes were immersed in the solutions for 3 h, taking the moment of immersion as zero time. Then, impedance measurements at open-circuit potential were made using a sinusoidal signal of 10 mV amplitude and frequencies in the 0.01 Hz-100 kHz range. Cathodic and anodic polarization was then carried out potentiodynamically with 1 mV s^{-1} sweep rate. After each run, the samples were reground with emery paper to a 1200-grit finish in order to remove any product formed on the metal surface which could affect the following tests, rinsed with distilled water and dried.

3. Results and Discussion

3.1. *Microstructure of HA/316L stainless steel biocomposites*

Figure 1 shows micrographs of polished surfaces of the investigated materials obtained by scanning electron microscopy (SEM). The microstructure of sintered 316L presents austenitic grains and pores (black spots) (Figure 1a). The microstructure of 5% HA-316L composite is constituted of austenitic grains (grey regions), HA (light regions), an eutectic phase at the grains boundaries (represented by E letter) and pores (Figure 1b). The eutectic phase was also observed by Szewczyk-Nykiel[10]. It can be observed that HA was partially removed during grinding, leaving many holes. The chemical analysis by energy dispersive spectroscopy (EDS) of the austenitic grains in 5% HA-316L composite (P2 and P3-Figure 1b) showed the presence of the constituent elements of 316L stainless steel, Fe, Cr, Ni and Mo and some trace of P (Table 1). P element is not found in sintered 316L steel (P1-Figure 1a). This means that some phosphorus diffused from HA phase into austenitic grains during sintering of the composites[10]. In the light regions (P4 and P5-Figure 1b), large amount of Ca and O are present, as well as Fe and Cr (Table 1). Thus, it seems that Cr and Fe have migrated from austenitic phase. The eutectic phase (P6-Figure 1b) contains significative amounts of Fe, Cr, Mo, Ni and P and some trace of Ca (Table 1), and can be the result of some chemical reaction occured during sintering.

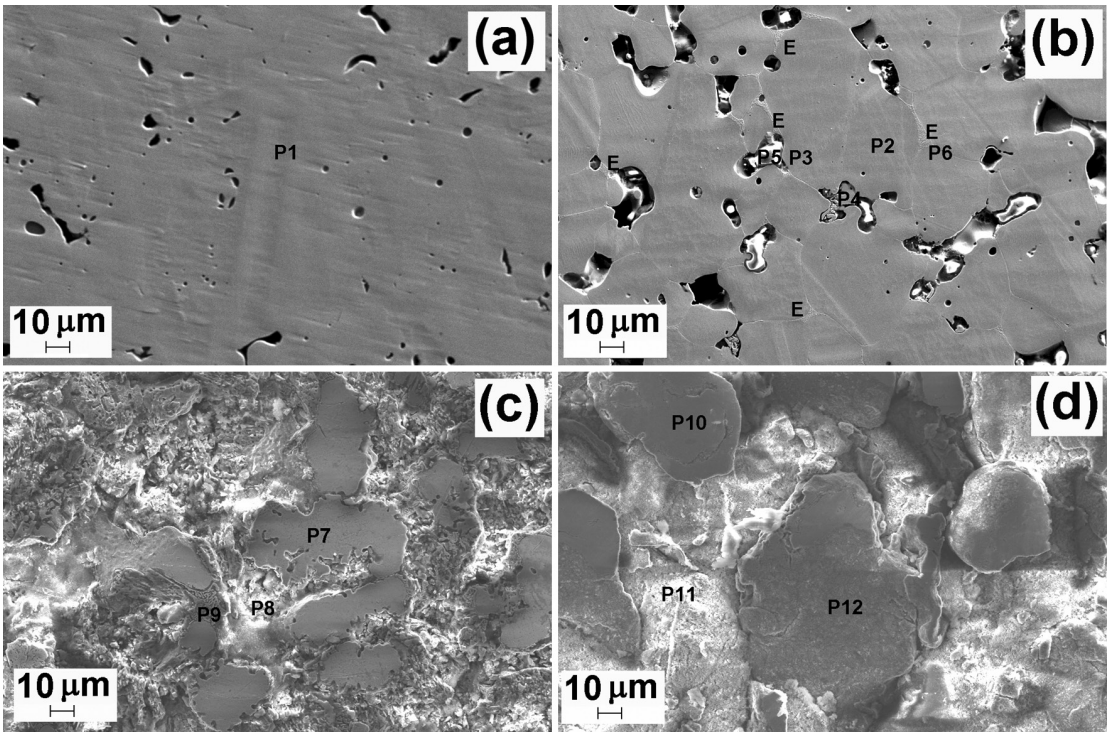

Figure 1. Microstructure of sintered (a) 316L stainless steel, (b) 5% HA-316L, (c) 20% HA-316L and (d) 50% HA-316L composites.

Table 1. Microanalysis by EDS of sintered 316L and HA-316L composites (wt. (%)).

Material / Region		Element						
		Fe	**Cr**	**Ni**	**Mo**	**P**	**Ca**	**O**
316L	P1-Figure 1a	66.2	17.9	13.7	2.2	-	-	-
	P2-Figure 1b	66.6	17.7	13. 6	1.7	0.4	-	-
5%HA-316L	P3-Figure 1b	66.3	17.9	13.3	2.0	0.5	-	-
	P4-Figure 1b	3.4	2.8	-	-	-	25.0	68.8
	P5-Figure 1b	0.8	26.7	-	-	-	31.3	41.2
	P6-Figure 1b	47.3	27.1	10.1	7.9	7.4	0.2	-
	P7-Figure 1c	76.2	8.1	14.9	-	0.8		
20%HA-316L	P8-Figure 1c	10.8	16.5	2.6	-	-	10,0	60.1
	P9-Figure 1c	30.8	18.9	8.0	7.6	16.5	2.5	15.7
	P10-Figure 1d	69.2	17.0	13.7	-	0.1	-	-
50%HA-316L	P11-Figure 1d	3.5	1.7	-	-	17.6	35.6	41.6
	P12-Figure 1d	47.4	24.0	8.7	-	1.0	2.8	16.1

Phosphorus has also diffused from HA phase into austenitic grains during sintering of the 20% and 50% HA-316L composites (P7-Figure 1c and P10-Figure 1d, Table 1). In the 50% HA-316L composite some steel grains are rich in Ca and O too (P12-Figure 1d, Table 1) and in the HA regions, besides the presence of Ca, P and O, Fe and Cr were also detected (P11-Figure 1d, Table 1). This could be related to some reaction between 316L steel and HA during sintering[7]. Similarly, in the HA regions of the 20% HA-316 composite, Fe, Cr and Ni are present (P8-Figure 1c, Table 1). Some regions with high concentrations of Fe, Cr, Ni, Mo, Ca, P and O and that look like an eutectic phase (E) were also observed in the 20% HA-316L composites (P 9-Figure 1c, Table 1).

Besides diffusion, possible phase transformation during sintering could be considered. The X ray diffraction patterns of 316L and composite samples only revealed the peaks of the austenite phase (JCPDS card number 33-0397)[15], and also peaks of HA (JCPDS card number 09-0432)[15] for the composites, which attests that the austenite phase did not undergoe transformation during sintering.

3.2. *Corrosion behavior of HA/316L biocomposites in Ringer's solution*

The open-circuit potentials (OCPs) of 316L and HA/316L composites tended to stabilize before 3 h immersion in Ringer's solution (Figure 2). The values of all OCPs are found in the stability regions of Fe_2O_3 and Cr_2O_3 of the Fe-H_2O and Cr-H_2O Pourbaix' diagrams[16], which shows the passive behavior of all materials. The OCPs values measured at 3 h (E_{corr} corrosion potentials) shifted in the negative direction as the HA content increased (Table 2), which means that the addition of HA turned the materials less noble. Tulinski[13] found the same tendency for HA (0, 5, 10 and 15 wt.%) -nickel free stainless steel composites in Ringer's solution.

The polarization curves of 316L stainless steel and HA-316L composites in Ringer's solution at room temperature are presented in Figure 3. The shape of the curves is very similar for all materials, which shows that the anodic and cathodic reactions occurring on the different surfaces

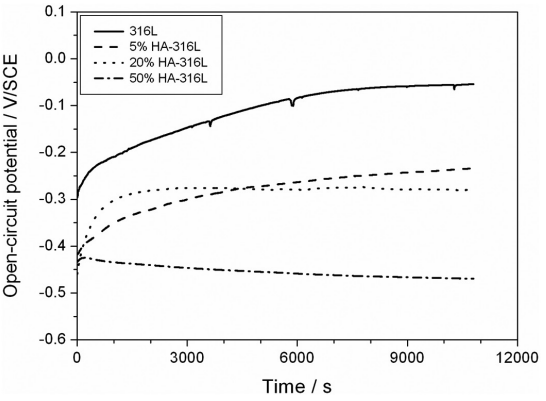

Figure 2. Variation of open-circuit potential with time for sintered 316L stainless steel and HA-316L composites in Ringer's solution at room temperature.

are identical. The cathodic domain is related first to the reduction of dissolved oxygen and at lower potentials to the simultaneous reduction of water. The anodic branch presents a pseudo-plateau corresponding to the passive region. It was shown that the passive film on 316 stainless steel is mainly constituted of chromium oxide and lower contents of iron and molybdenum oxides, without presence of nickel oxide[17]. For higher potentials the anodic current density increases strongly due to the breaking of passivity related to pitting corrosion.

Nevertheless, the anodic and cathodic current densities increase as the HA content in the composites increases.

Accordingly to the variation of E_{corr} values, the null-current potential $E_{i=0}$ shifted in the negative direction as the HA content increased (Figure 3 and Table 2). The $E_{i=0}$ values are more negative than the E_{corr} ones, which may be due to the partial removal of oxide passive film during the cathodic polarization.

The corrosion current density i_{corr} determined by extrapolation of the cathodic Tafel lines to the null-current potential are reported in Table 2 for the four materials. A significant decrease in corrosion resistance is observed for

Table 2. Corrosion potential (E_{corr}), null-current potential ($E_{i=0}$), breakdown potential (E_b), corrosion current density (i_{corr}), passive current density (i_{pass} measured at the middle of the passive region) and impedance modulus ($|Z|$ measured at 0.01 Hz) of sintered 316L stainless steel and HA-316L composites in Ringer's solution at room temperature.

	316L	5%HA-316L	20%HA-316L	50%HA-316L
E_{corr} / V/SCE	–0.054 ± 0.008	–0.229 ± 0.012	–0.304 ± 0.025	–0.488 ± 0.029
$E_{i=0}$ / V/SCE	–0.173 ± 0.025	–0.398 ± 0.018	–0.516 ± 0.024	–0.659 ± 0.041
E_b / V/SCE	0.376 ± 0.033	0.214 ± 0.019	–0.080 ± 0.043	–0.107 ± 0.006
i_{corr} / A cm^{-2}	(1.8 ± 0.4) × 10^{-7}	(6.7 ± 1.2) × 10^{-7}	(22.2 ± 0.8) × 10^{-7}	(31.0 ± 3.5) × 10^{-7}
i_{pass} / A cm^{-2}	(2.05 ± 0.30) × 10^{-6}	(1.21 ± 0.03) × 10^{-6}	(5.06 ± 0.49) × 10^{-6}	(14.20 ± 4.6) × 10^{-6}
$\|Z\|_{f=0.01\ Hz}$ / kΩ cm^2	111.0 ± 23.4	113.7 ± 8.3	11.1 ± 3.8	7.6 ± 2.5

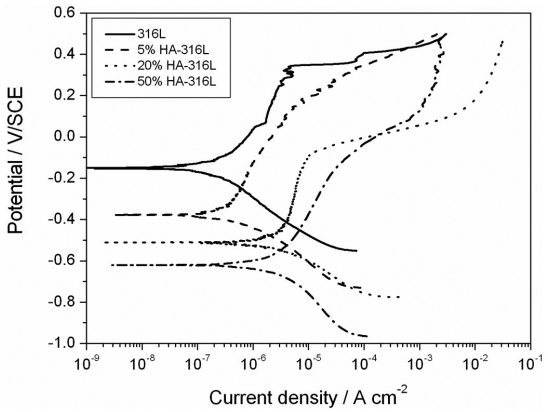

Figure 3. Polarization curves of sintered 316L stainless steel and HA-316L composites in Ringer's solution at room temperature.

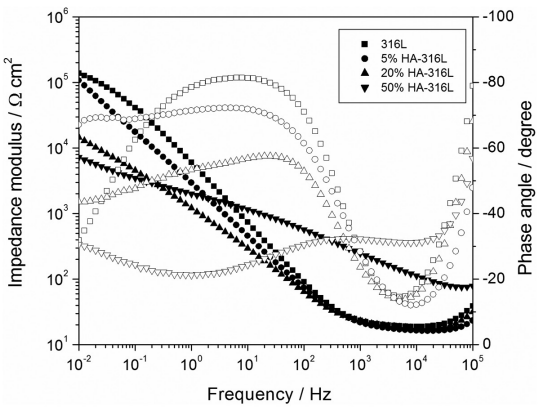

Figure 4. Bode diagrams of sintered 316L stainless steel and HA-316L composites in Ringer's solution at room temperature and at corrosion potential.

the 20 and 50 % HA-316L composites. This may be related to the enrichment of HA phase with Cr. Nevertheless, the corrosion current densities are in the order of 10^{-6} A cm^{-2} or less for all materials, which is characteristic of corrosion resistant materials. Tulinski[13] showed that the corrosion resistance of HA-nickel free stainless steel composites increases with increasing HA content between 0 and 10% but further decreases for 15% HA-SS composite.

The passive current density i_{pass} measured for 20 and 50% HA-316L composites is also higher than that obtained for 316L steel and 5% HA-316L composite which depicts a lower protective character of their passive film (Table 2).

The breakdown potential E_b (measured when the anodic current density suddenly increases) shifts in the negative direction as the HA content increases, which is characteristic of a higher susceptibility to pitting (Table 2).

The values of E_{corr}, i_{corr}, i_{pass} and E_b for 316L steel are close to the values obtained by Talha[18] in Ringer's solution containing $NaHCO_3$ at 37 °C.

The spontaneous corrosion behavior of metals and alloys is better evaluated from the impedance measurements at corrosion potential. Indeed, the use of this technique only disturbs the potential from +10 mV to –10 mV around the spontaneous corrosion potential. Thus, during the measurements, the electrode surface is only slightly changed.

Figure 4 shows the Bode diagrams obtained for 316L stainless steel and HA-316L composites in Ringer's solution at corrosion potential. For 316L stainless steel, the impedance diagram presents one time constant. The slope of log (Impedance) versus log (Frequency) is close to –1 and the phase angle close to –90° on a large frequency range, which is characteristic of passive material. For the HA-316L composites, Bode diagrams with two time constants were obtained. Only the 5% HA-316L composite maintains a behavior close to that of 316L steel, i.e. high impedance values, slope of log (Impedance) versus log (Frequency) close to –1 and a phase angle around –70° on a large frequency range.

The corrosion resistance of the materials can be estimated for comparison by the values of impedance modulus at low frequencies (Table 2). 316L stainless steel and 5% HA-316L composite present values close to 10^5 Ω cm^2 and 20 and 50% HA-316L composites values around 10^4 Ω cm^2.

Though there is a clear evidence that corrosion resistance decreases with increasing HA content, the values of i_{corr}, i_{pass} and Z (at low frequencies) must be considered carefully. Indeed, the porosity of the composites also increases with increasing HA content (Figure 1), which can lead to a significant error on the measured sample area exposed to the corrosive medium, and consequently to an error on i_{corr}, i_{pass} and Z values.

3.3. *Corrosion behavior of HA/316L biocomposites in 0.1M HCl solution*

The open-circuit potentials (OCPs) of 316L and HA-316L composites also stabilized before 3 h immersion in 0.1M HCl solution (Figure 5). The values of all OCPs are found in the stability regions of Fe^{2+} and Cr^{3+} ions of the Fe-H_2O and Cr-H_2O Pourbaix' diagrams[16], which depicts the active behavior of all materials. The OCPs values measured at 3 h (corrosion potentials) shifted in the negative direction as the HA content increased (Table 3), which means that the addition of HA also turned the materials more active in HCl solution. It can be noted that the corrosion potentials of both 316L and 5% HA-316L composite are very close. The same occurred for both 20% and 50% HA- 316L composites. The E_{corr} values are generally more negative than those measured in Ringer's solution, which shows that the materials are less noble in HCl solution.

The polarization curves of 316L stainless steel and HA-316L composites in 0.1M HCl solution at room temperature are shown in Figure 6. The cathodic branches are related to hydrogen evolution. It seems that the kinetics of H^+ reduction on 316L steel is controlled by activation but is diffusion-controlled on the HA-316L composites. The anodic curves present different shapes. 316L steel showed a narrow passive region between nearly –0.260 and –0.160 V/SCE followed by the film breakdown above –0.160 V/SCE. For the 5% HA-316L composite, the cathodic polarization seems to have led to the dissolution of the passive film since during the anodic polarization, the curve presented an anodic peak followed by a wide passive region between –0.150 and 0.150 V/SCE. The corrosion and passive current densities are similar for both 316L and 5% HA-316L composite (Table 3). Nevertheless, the passive film on the 5% HA-316L surface only undergoes pitting corrosion for potentials above 0.150 V/SCE. The anodic branches for both 20 and 50% HA-316L composites are very similar. Both materials are active and no passivation is observed. Thus E_b and i_{pass} values

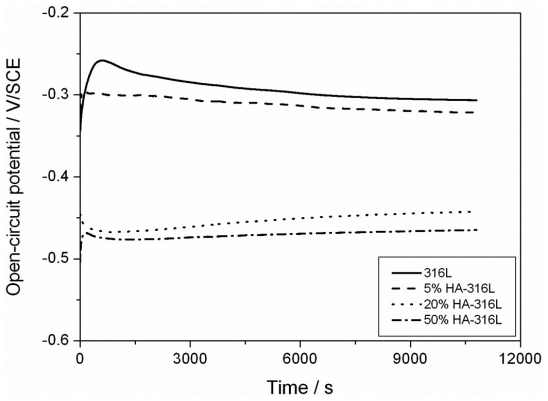

Figure 5. Variation of open-circuit potential with time for sintered 316L stainless steel and HA-316L composites in 0.1M HCl solution at room temperature.

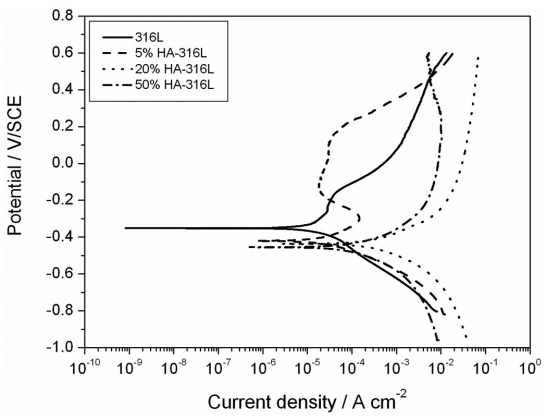

Figure 6. Polarization curves of sintered 316L stainless steel and HA-316L composites in 0.1M HCl solution at room temperature.

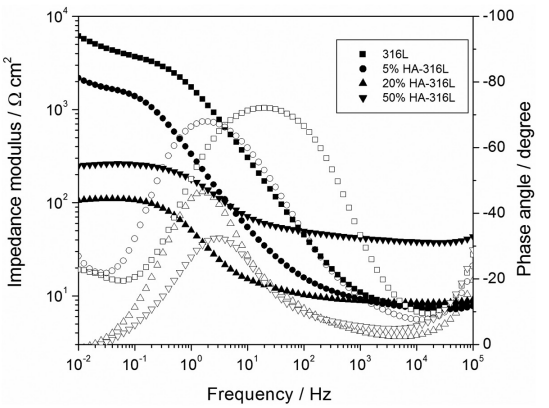

Figure 7. Bode diagrams of sintered 316L stainless steel and HA-316L composites in 0.1M HCl solution at room temperature and at corrosion potential.

Table 3. Corrosion potential (E_{corr}), null-current potential ($E_{i=0}$), breakdown potential (E_b), corrosion current density (i_{corr}), passive current density (i_{pass} measured at the middle of the passive region) and impedance modulus ($|Z|$ measured at 0.01 Hz) of sintered 316L stainless steel and HA-316L composites in 0.1M HCl solution at room temperature.

	316L	5%HA-316L	20%HA-316L	50%HA-316L
E_{corr} / V/SCE	–0.310 ± 0.006	–0.332 ± 0.015	–0.442 ± 0.001	–0.462 ± 0.002
$E_{i=0}$ / V/SCE	–0.359 ± 0.012	–0.424 ± 0.006	–0.435 ± 0.001	–0.456 ± 0.002
E_b / V/SCE	–0.158 ± 0.012	0.156 ± 0.005	*	*
i_{corr} / A cm^{-2}	(2.3 ± 0.4) × 10^{-5}	(5.0 ± 2.0) × 10^{-5}	(42.0 ± 11.3) × 10^{-5}	(21.0 ± 2.8) × 10^{-5}
i_{pass} / A cm^{-2}	(3.1 ± 0.4) × 10^{-5}	(4.6 ± 2.5) × 10^{-5}	*	*
$\|Z\|_{f=0.01\ Hz}$ / Ω cm^2	5469 ± 962	1580 ± 840	98 ± 10	295 ± 66

*no passive region and consequently no breakdown are observed for 20 and 50% HA-316L composites.

are not available for these materials. Their corrosion current densities are one order of magnitude higher than the values measured for 316L and 5% HA-316L composite (Table 3).

Figure 7 shows the Bode diagrams obtained for 316L stainless steel and HA-316L composites in 0.1M HCl solution at corrosion potential. Both 316L stainless steel and 5% HA-316L composite show a slope of log (Impedance) versus log (Frequency) close to –1 and a phase angle near –70° in the intermediary frequency range frequency range.

The corrosion resistance of the materials can be estimated by the values of impedance modulus at low frequencies (Table 3). 316L stainless steel and 5% HA-316L composite present values in the order of 10^3 Ω cm^2 and 20 and 50% HA- 316L composites values around 10^2 Ω cm^2.

4. Conclusions

Sintered 316L stainless steel and 5, 20 and 50 wt. (%) HA-316L composites are passive in Ringer's solution and active in 0.1M HCl solution which simulates occluded cell corrosion conditions.

The corrosion resistance decreases with increasing HA content in both solutions.

Sintered 316L stainless steel and 5, 20 and 50 wt. (%) HA-316L composites are highly corrosion resistant in Ringer's solution.

Only 316L stainless steel and 5 wt. (%) HA-316L composite can be considered corrosion resistant in 0.1M HCl solution.

References

1. Stainless Steels. 3rd ed. Materials Park: ASM International; 1999.
2. Javidi M, Javadpour S, Bahrololoom ME and Ma J. Electrophoretic deposition of natural hydroxyapatite on medical grade 316L stainless steel. *Materials Science and Engineering C*. 2008; 28:1509-15. http://dx.doi.org/10.1016/j.msec.2008.04.003
3. Gopi D, Prakash V, Collins A and Kavitha L. Evaluation of hydroxyapatite coatings on borate passivated 316L SS in Ringer's solution. *Materials Science and Engineering C*. 2009; 29:955-8. http://dx.doi.org/10.1016/j.msec.2008.08.020
4. Javidi M, Bahrololoom ME, Javadpour S and Ma J. In vitro electrochemical evaluation and phase purity of natural hydroxyapatite coating on medical grade 316L stainless steel. *Materials and Corrosion*. 2009; 60:336-43. http://dx.doi.org/10.1002/maco.200805117
5. Aksakal B, Gavgali M and Dikici B. The Effect of Coating Thickness on Corrosion Resistance of Hydroxyapatite Coated $Ti_6A_{l4}V$ and 316L SS Implants. *Journal of Materials Engineering and Performance*. 2010; 19:894-9. http://dx.doi.org/10.1007/s11665-009-9559-7
6. Miao X. Observation of microcracks formed in HA-316L composites. *Materials Letters*. 2003; 57:1848-53. http://dx.doi.org/10.1016/S0167-577X(02)01080-7
7. Zou J, Ruan J, Huang B, Liu J and Zhou X. Physico-chemical properties and microstructure of hydroxyapatite-316L stainless steel biomaterials. *Journal of Central South University of Technology*. 2004; 11:113-8. http://dx.doi.org/10.1007/s11771-004-0024-3
8. Guo HB, Miao X, Chen Y, Cheang P and Khor KA. Characterization of hydroxyapatite– and bioglass–316L fibre composites prepared by spark plasma sintering. *Materials Letters*. 2004; 58:304-7. http://dx.doi.org/10.1016/S0167-577X(03)00474-9
9. Fan X, Chen J, Zou J, Wan Q, Zhou Z and Ruan J. Bone-like apatite formation on HA/316L stainless steel composite surface in simulated body fluid. *Transactions of Nonferrous Metals Society of China*. 2009; 19:347-52. http://dx.doi.org/10.1016/S1003-6326(08)60276-9
10. Szewczyk-Nykiel A and Nykiel M. Study of hydroxyapatite behavior during sintering of 316L steel. *Archives of Foundry Engineering*. 2010; 10:235-40.
11. Fontana MG. *Corrosion Engineering*. New York: MacGraw-Hill Book Company; 1986.
12. Tulinski M and Jurczyk M. Corrosion resistance of nickel-free austenitic stainless steels/hydroxyapatite composites. *Physica Status Solidi C*. 2010; 7:1359-62. http://dx.doi.org/10.1002/pssc.200983351
13. Tulinski M and Jurczyk M. Corrosion resistance of nickel-free austenitic stainless steels and their nanocomposites with hydroxyapatite in Ringer's solution. *Materials Science Forum*. 2011; 674:159-63. http://dx.doi.org/10.4028/www.scientific.net/MSF.674.159
14. Silva G, Baldissera MR, Trichês ES and Cardoso KR. Preparation and characterization of stainless steel 316L/HA biocomposite. *Materials Research*. 2013; 16(2):304-309. http://dx.doi.org/10.1590/S1516-14392012005000182
15. International Centre for Diffraction Data. *JCPDS-ICDD, PCPDFWIN version 2.1*. Swarthmore; 2000.
16. Pourbaix M. *Atlas of Electrochemical Equilibria in Aqueous Solutions*. Oxford: Pergamon Press; 1966.
17. Olsson COA and Landolt D. Passive films on stainless steels- Chemistry, structure and growth. *Electrochimica Acta*. 2003; 48:1093-104. http://dx.doi.org/10.1016/S0013-4686(02)00841-1
18. Talha M, Behera CK and Sinhá OP. Potentiodynamic polarization study of Type 316L and 316LVM stainless steels for surgical implants in simulated body fluids. *Journal of Chemical Pharmaceutical Research*. 2012; 4:203-8.